

Correlating Space, Wavelength, and Polarization of Light: Spatiospectral Vector Beams

Lea Kopf,* Rafael Barros,* and Robert Fickler*

Cite This: <https://doi.org/10.1021/acsp Photonics.3c01322>

Read Online

ACCESS |



Metrics & More



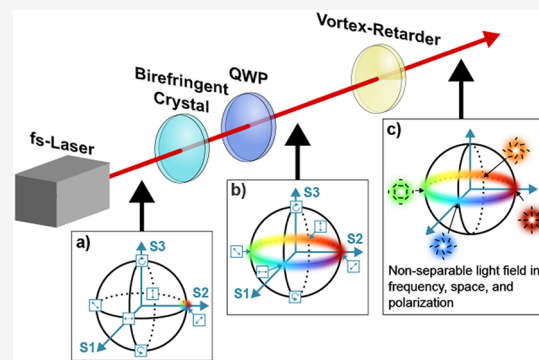
Article Recommendations



Supporting Information

ABSTRACT: Increasing the complexity of a light field through the advanced manipulation of its degrees of freedom (DoFs) provides new opportunities for fundamental studies and technologies. Correlating polarization with the light's spatial or spectral shape results in so-called spatial or spectral vector beams that are fully polarized and have a spatially or spectrally varying polarization structure. Here, we extend the general idea of vector beams by combining both approaches and structuring a novel state of light in three nonseparable DoFs, i.e., space, wavelength, and polarization. We study in detail their complex polarization structure, show that the degree of polarization of the field is only unveiled when the field is narrowly defined in space and wavelength, and demonstrate the analogy to the loss of coherence in nonseparable quantum systems. Our work extends the toolbox of structured light and might inspire new applications benefiting from the quantum-like features of nonseparable light fields.

KEYWORDS: vector beam, nonseparability, pulse-shaping, structured light



INTRODUCTION

Increasing the complexity of a light field and the control of different degrees of freedom (DoFs) is beneficial for advancing research and technology. Increasingly complex structures realized by combining several DoF's have been studied in a myriad of experiments over the last decades, and the enhanced understanding of the interplay of the DoFs has already enabled novel photonic technologies.^{1–6} Initially, many experiments have studied structuring transverse light fields and shaping the temporal profile of pulses, both in their scalar forms, i.e., with a uniform polarization structure.^{7,8} The complexity of the light field's structure was further increased by including the polarization domain, leading to beams with spatially nonuniform polarization distributions, i.e., spatial vector beams, as well as a temporally varying polarization vector across the pulse duration. Over the last years, this approach has been extended to combine all DoFs, e.g., the study of advanced spatiotemporal pulses of vectorial light fields,⁹ or the adaptation of established concepts such as complex transverse spatial fields to the spatiotemporal domain.^{10,11} Interestingly, the focus in most of the research efforts has been to generate complex polarization and spatial patterns over the temporal domain of light with much less attention to studying structured light fields in the time's complementary DoF, i.e., the spectral domain. Correlating polarization with the wavelength of a light pulse, for example, can be used for advanced sensing and pulse characterization schemes.^{12–16}

Here, we extend the idea of spatial and spectral vector beams by combining all three DoFs, namely, polarization, space, and wavelength of the light field. We term such light pulses spatiospectral vector beams (SSVBs), which are light fields with a varying polarization structure in space as well as wavelength as shown in Figure 1a. Using a simple setup consisting of only three optical elements placed along a single beamline, we are able to generate highly complex pulses of light for which any given wavelength (or transverse angular position) shows a different spatial (or spectral) polarization pattern. We further show that all three DoFs are nonseparable, and the complex vectorial nature of the light field can only be observed when all DoFs are resolved. By integration over the light's transverse spatial extent or wavelength spectrum (or both), the beam would be seemingly unpolarized. Finally, we detail the analogy of such complex structured light fields to a tripartite Greenberger–Horne–Zeilinger (GHZ) state, where the DoFs of the classical light field play the role of the different quantum particles in the GHZ description.

Received: September 15, 2023

Revised: November 21, 2023

Accepted: November 28, 2023

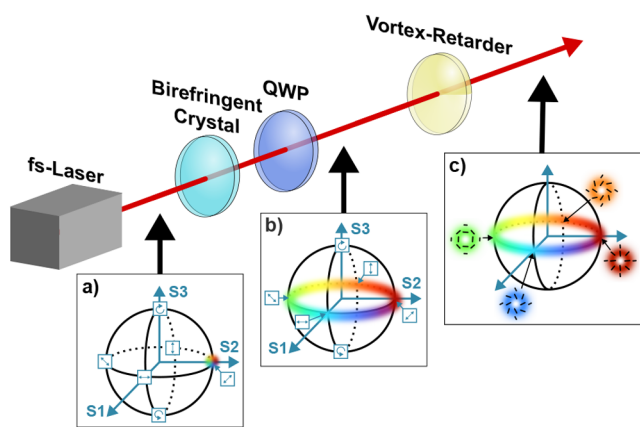


Figure 1. Conceptual idea. A simple generation scheme consisting only of a birefringent crystal, a quarter-wave plate (QWP), and a vortex-retarder generates a complex light field where polarization, wavelength, and space are correlated. The colors in the insets symbolize the different wavelength components of the light field. (a) Poincaré sphere displaying that the light field is diagonally polarized. (b) Poincaré sphere of the light field shows that each wavelength component has a different linear polarization. (c) The higher-order Poincaré sphere^{17,18} illustrates that each wavelength has a different spatial polarization pattern.

METHOD

We consider an SSVB of the form

$$\vec{E}(\vec{r}, \lambda) = \sqrt{\frac{I_0}{2}} [S_1(\vec{r})F_1(\lambda)\hat{e}_1 + S_2(\vec{r})F_2(\lambda)\hat{e}_2] \quad (1)$$

where \vec{r} is the position vector, λ is the wavelength, I_0 is the total field intensity, $S_{1,2}$ and $F_{1,2}$ are normalized spatial and spectral basis functions, respectively, and $\hat{e}_{1,2}$ are unit polarization vectors. We assume orthogonal polarization vectors with $\hat{e}_i \cdot \hat{e}_j = \delta_{ij}$, but allow for the spatial and spectral functions to have nonvanishing overlap. Thus, the function can describe a light field with nonseparable polarization, space, and wavelength for zero overlap.

As a measure of the degree of tripartite nonseparability of field (eq 1), we consider the degree of polarization (DoP) of the light field. As we detail in the Supporting Information,¹⁹ the DoP is given by

$$D = \sqrt{\frac{(\Lambda_{11}^S \Lambda_{11}^F - \Lambda_{22}^S \Lambda_{22}^F)^2 + 4|\Lambda_{12}^S|^2 |\Lambda_{12}^F|^2}{(\Lambda_{11}^S \Lambda_{11}^F + \Lambda_{22}^S \Lambda_{22}^F)^2}} \quad (2)$$

where $\Lambda_{ij}^S = \langle S_i, S_j \rangle_{\Omega_S}$ and $\Lambda_{ij}^F = \langle F_i, F_j \rangle_{\Omega_F}$ ($j = 1, 2$) are the inner products between the spatial and spectral basis functions over finite regions Ω_S and Ω_F in space and wavelength, respectively. Experimentally, the DOP can be retrieved from the Stokes parameters resulting from intensity measurements integrated over Ω_S and Ω_F .

Note that when integrating over the complete spatial and spectral DoFs ($\Omega_S = \mathbb{R}^2$ and $\Omega_F = \mathbb{R}$), eq 2 yields $D = |\Lambda_{12}^S \Lambda_{12}^F|$. Thus, when either the spatial or the spectral basis functions are orthogonal, the measured light field is seemingly unpolarized. The same argument holds for space- or wavelength-only measurements, which yield reduced degrees of spatial and spectral coherence, respectively. Only joint measurements of the three DoFs unveil the full coherence of the input field, which is a signature of tripartite nonseparability. The apparent decoher-

ence of the field (eq 1) upon partial tracing of one DoF is a byproduct of its mathematical similarity to the GHZ states.^{20–22} Classically, such a tripartite nonseparable behavior can also be explained in an intuitive way. At any point in space where both spatial basis functions are nonvanishing, the polarization is spectrally nonuniform, i.e., a spectral vector beam.¹⁵ Similarly, at any wavelength present in both spectral basis functions, the polarization is spatially nonuniform, i.e., a spatial vector beam.²³ Lastly, measuring the linear polarization state of the light field leads to a strong correlation between spatial and spectral structures. In other words, specifying one DoF can project the remaining two in a bipartite nonseparable field, which we will explore in more detail in the Results section. We note that a related behavior has been observed using multiple beams, each with a spatially varying polarization.²⁴

Experimental Generation. To create an SSVB, we use the process shown in Figure 1. First, Fourier-limited laser pulses with a duration of $\tau = 220$ fs and centered at a wavelength of 780 nm are linearly polarized. The polarization is chosen to be diagonal with respect to the fast and slow axes of a 2 mm long birefringent BaB₂O₄ (BBO) crystal with the optical axis oriented 23.4° from the propagation direction. The propagation through the birefringent crystal coherently splits each pulse into two trailing pulses with equal intensities, linearly polarized along the crystal's fast (*f*) and slow (*s*) axes, producing a spectral vector beam.¹⁵ The field at this stage is

$$\vec{E}(\vec{r}, \lambda) = \sqrt{\frac{I_0}{2}} S_0(\vec{r}) F_0(\lambda) [e^{i\pi c \delta t / \lambda} \hat{e}_f + e^{-i\pi c \delta t / \lambda} \hat{e}_s] \quad (3)$$

where $S_0(\vec{r})$ is a Gaussian transverse spatial profile, $F_0(\lambda)$ is the spectral function, c is the speed of light, and δt is the birefringent time delay. A subsequent quarter-wave plate oriented at 45° with respect to the fast axis of the crystal transforms the field's polarization components \hat{e}_f and \hat{e}_s to left and right circular polarizations, i.e., \hat{e}_R and \hat{e}_L , respectively. We set the time delay to $\delta t \approx \tau$ by choosing the appropriate crystal length and fine-tuning the crystal rotation, which ensured that the resulting linear polarization state in the wavelength domain rotates approximately once within one spectral bandwidth. This beam is nonseparable in wavelength and polarization, but still has only a single transverse structure, i.e., a Gaussian mode.

Next, we correlate the spatial DoF with polarization using an $m = 1$ zero-order vortex half-wave retarder. The vortex retarder has a constant half-wave retardance across the clear aperture with the fast axis oriented along $\theta = \phi/2$, where ϕ is the azimuthal angle. Upon transmission, the left and right circular polarization components change their handedness and acquire an azimuthally varying phase from 0 to 2π ,²⁵ resulting in

$$\vec{E}(\vec{r}, \lambda) = \sqrt{\frac{I_0}{2}} S_0(\vec{r}) F_0(\lambda) [e^{i\phi} e^{i\pi c \tau / \lambda} \hat{e}_L + e^{-i\phi} e^{-i\pi c \tau / \lambda} \hat{e}_R] \quad (4)$$

The field (eq 4) is exactly of the intended form of the SSVB (eq 1), provided that we identify $S_{1,2}(\vec{r}) = S_0(\vec{r}) e^{\pm i\phi}$ and $F_{1,2}(\lambda) = F_0(\lambda) e^{\pm i\pi c \tau / \lambda}$. Note that while the spatial basis functions are mutually orthogonal ($\langle S_1, S_2 \rangle_{\mathbb{R}^2} = 0$), the overlap between the spectral basis functions is nonvanishing ($\langle F_1, F_2 \rangle_{\mathbb{R}} \sim 1/e^2$). The spectral overlap limits the quality of our SSVB and is the cost of the simple method to produce it. We note that the aforementioned limitation can be overcome by more advanced pulse-shaping techniques to generate orthogonal temporal or

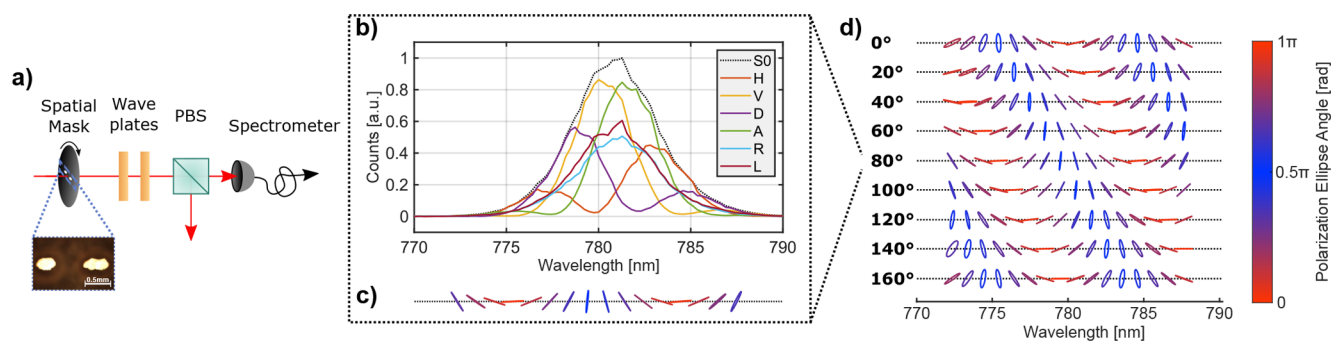


Figure 2. Spectrally resolved measurements of the generated SSVBs. (a) The measurement setup filters space by using a spatial mask. The inset shows a microscope image of the center of the slit mask made from black cardboard by using a simple laser cutter. Subsequently, it filters polarization using a half- and quarter-wave plate followed by a polarizing beam splitter (PBS). The final data acquisition is done in the spectral domain using a spectrometer. (b) Polarization-resolved spectral measurements with a spatial mask rotation angle of 80° . The letters “H”, “V”, “D”, “A”, “R”, and “L” refer to the measurements corresponding to the projection on horizontal, vertical, diagonal, antidiagonal, left-circular, and right-circular polarizations, respectively. (c) Reconstructed polarization ellipses over wavelength. The colors refer to the polarization ellipse rotation angle and are included for better visibility of the changes in polarization. (d) SSVB at different spatial mask rotation angles.

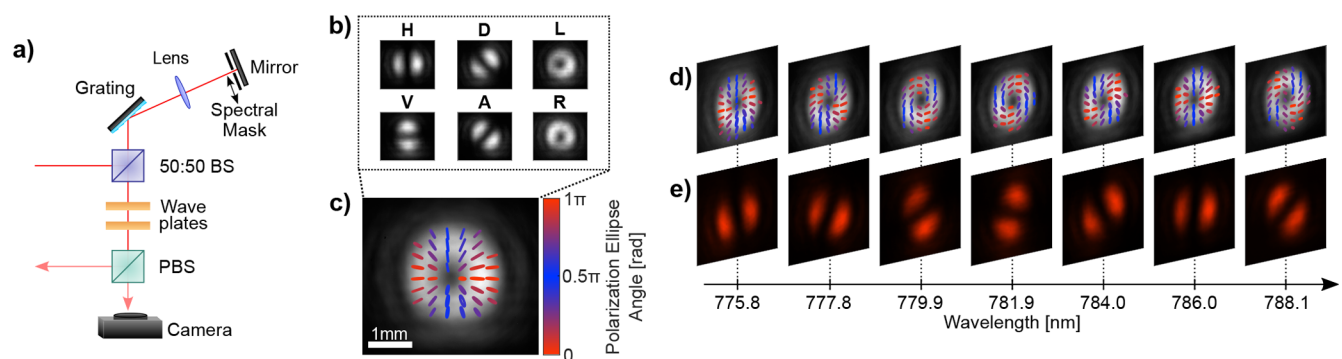


Figure 3. Spatially resolved measurements of the generated SSVB. (a) The measurement setup filters wavelength and polarization using a monochromator, wave plates, and a polarizing beam splitter (PBS). The data are acquired in the spatial domain with a camera. (b) Polarization measurements at a wavelength filter centered at 785.5 nm . The letters “H”, “V”, “D”, “A”, “R”, and “L” refer to the measurements corresponding to the projection on horizontal, vertical, diagonal, antidiagonal, left-circular, and right-circular polarizations, respectively. (c) Reconstructed SSVB from the polarization measurements shown in (b). The color corresponds to the rotation angle of the polarization ellipses and acts as a guide for the eye. (d) The SSVBs at varying wavelength filter positions. (e) Projection of the vector beam on the horizontal polarization at varying wavelength filter positions.

spectral modes;^{7,26} however, they lead to the same arguments as presented here.

RESULTS AND DISCUSSION

Characterization. To characterize the SSVB (eq 4), we performed both individual and joint measurements of its polarization, wavelength, and spatial profile. In the first set of measurements, we used the experimental setup depicted in Figure 2a). We send the SSVB through a spatial mask comprising two diametrically opposite 0.2 mm wide apertures centered at the azimuthal angles ϕ_p and $\phi_p + \pi$, which roughly corresponds to two 17° wide slits and projects the field onto approximately $\vec{E}(\phi_p, \lambda)$.

We characterize the resulting field with spectrally resolved polarization tomography, where the Stokes parameters are measured with a spectrometer, as shown for $\phi_p = 80^\circ$ in Figure 2b with the corresponding wavelength-dependent polarization ellipses in Figure 2c. In Figure 2d, we show different rotation angles of the spatial mask, which display a linear shift of the spectral-polarization structure. Note that the measured polarization states shown in Figure 2c,d) are not strictly linear, as expected from eq 4, but consist of elongated ellipses. This results from the nonzero overlap of the spectral basis functions in our

scheme and experimental imperfections such as the finite area of the spatial slits.

In the second set of measurements, we project the SSVB onto wavelength instead of space using the setup depicted in Figure 3a. A monochromator consisting of a diffraction grating, a mirror, and a tunable rectangular slit selects a central wavelength λ_p , which projects the field onto approximately $\vec{E}(\vec{r}, \lambda_p)$. The projection resolution is fixed by the minimum bandwidth of around 2.1 nm of the monochromator. We characterize the spectrally filtered field through spatially resolved polarization tomography in which the Stokes parameters are measured with a CMOS camera. In Figure 3b, we show the polarization-resolved images obtained at $\lambda_p = 785.5\text{ nm}$ with the corresponding spatial vector beam in Figure 3c. The spatial vector beams retrieved for different wavelengths are shown in Figure 3d, and, to help visualize the wavelength dependence of the retrieved field structures, the related images obtained at a fixed horizontal polarization are additionally shown in Figure 3e. The polarized images show a two-lobe structure that rotates across the spectrum, as expected from eq 1.

We further study that partially resolving the spatial and spectral domains can be used to control the DoP of the laser beam. To this end, we performed polarization measurements for

different spatial and spectral bandwidths. We repeat the measurements shown in Figure 3a with different spectral resolutions at $\lambda_p = 779.75$ nm by changing the width of the rectangular slit in the monochromator. Then, a computational spatial mask with varying angular slit widths is added to the images in postprocessing, simulating the physical mask used in Figure 2a. From the measured Stokes parameters for each setting, we retrieve the DoP values shown in Figure 4. By

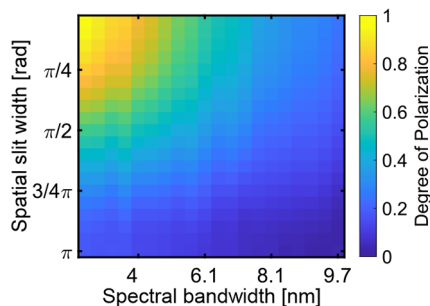


Figure 4. DoP as a function of the spatial and spectral filter bandwidths. As both filters are enlarged, the DoP decreases due to the nonseparability of space, wavelength, and polarization.

increasing the bandwidth of the wavelength filter or the slit width of the spatial mask, thereby averaging over the two DoFs, the beam's DoP decreases substantially. The initial DoP of 0.95, measured with a wavelength filter bandwidth of 2.1 nm and a spatial slit mask 0.16 rad wide, drops down to 0.04 when both wavelength and spatial filters are completely removed, showing excellent agreement with the simulations (see Supporting Information¹⁹). Without resolving all DoFs, we thus have a seemingly unpolarized light field. Moreover, note that the minimum DoP obtained for spatially resolved measurements is non-negligible (~ 0.2), which agrees with the estimated overlap between the spectral basis functions of $1/e^2$.

Analogy with Quantum Mechanics. As has been already recognized, classical nonseparable light fields share a mathematical similarity with entangled quantum states.^{27–29} In contrast to manifold discussions of two nonseparable DoFs of light and the analogy to Bell states,^{30,31} SSVBs are mathematically similar to the description of three-particle GHZ states. The GHZ state has the form

$$|\Psi\rangle = \frac{1}{\sqrt{2}}(|000\rangle + |111\rangle) \quad (5)$$

where $|0\rangle$ and $|1\rangle$ denote the two possible states of each quantum system expressed in terms of qubits in the computational or z basis. The mutually unbiased bases to z are the x and y bases, defined in the Dirac notation as $|\pm x\rangle = (|0\rangle \pm |1\rangle)/\sqrt{2}$ and $|\pm y\rangle = (|0\rangle \pm i|1\rangle)/\sqrt{2}$, respectively.

To demonstrate the nonseparability of the SSVB, we closely follow the GHZ argument,²¹ which focuses on the simultaneous measurements of all three qubits in the x basis (xxx measurement). In the original GHZ argument, the two possible measurement outcomes in each basis are ascribed to the values $+1$ and -1 . Together with the assumption of a local realistic theory, it is possible to show that classical correlations require the product of the measurement outcomes in the x basis to be $+1$, while for quantum correlations the outcome will be -1 . By adapting these ideas to SSVBs and showing a similar behavior,

we can use the GHZ argumentation to demonstrate the nonseparability of the classical light field.

We assign the notation in eq 5 to the SSVB by representing the spatial, spectral, and polarization modes as the first, second, and third entries of the state vector, respectively. For the spatial DoF, the z basis is formed by the spatial functions $S_{1,2}(\vec{r}) = S_0(\vec{r})e^{\pm i\phi}$, which contains counter-rotating spiral wavefronts carrying opposite orbital angular momenta,³² and indistinguishable intensity profiles. On the other hand, the x (y) basis modes have two-lobe structures oriented along 0° and 90° (45° and -45°)³³ and can be distinguished by narrow slits oriented along these directions.^{34,35} We implement these slits using the spatial mask already presented in the measurements of Figure 2.

In the wavelength domain, the z basis is formed by the spectral functions $F_{1,2}(\lambda) = F_0(\lambda)e^{\pm i\pi\tau c/\lambda}$, which cannot be distinguished by measurements of the spectral amplitude. On the other hand, the modes composing the x basis are $F_{1x} \propto F_0(\lambda)\cos(\pi\tau c/\lambda)$ and $F_{2x} \propto F_0(\lambda)\cos(\pi\tau c/\lambda - \pi/2)$, while those of the y basis are $F_{1y} \propto F_0(\lambda)\cos(\pi\tau c/\lambda - \pi/4)$ and $F_{2y} \propto F_0(\lambda)\cos(\pi\tau c/\lambda - 3\pi/4)$. In analogy to the spatial domain, we measure in the x and y bases by choosing, in postprocessing, four wavelengths spaced by $1/\tau$ at which the intensity difference between the horizontal/vertical or diagonal/antidiagonal polarization components is maximized.

Lastly, for the polarization DoF, we define the z basis vectors as the left and right circularly polarized components of the light field. Consequently, the x basis corresponds to horizontal/vertical linear polarizations, and the y basis corresponds to diagonal/antidiagonal linear polarizations. A graphical overview of the chosen bases is given in the Supporting Information.¹⁹

Figure 5 shows the measurement results for all terms of the normalized state (eq 5) written in the x and y bases. More information on the normalization procedure can be found in the Supporting Information.¹⁹ Clearly, the xxx measurements show that the product of the three outcomes mostly yields $+1$, with a small contribution of -1 due to experimental limitations and imperfections. We regard this result as an interesting way to show the nonseparability between polarization, spatial profile, and wavelength by exploring the mathematical isomorphism with the GHZ state.

CONCLUSION

In this article, we introduced and experimentally realized a light field with a complex polarization structure in space as well as wavelength: a spatio-spectral vector beam. Our measurements show that the SSVB is well-defined in its three DoFs if, and only if, they are measured jointly, while individual measurements result in apparent incoherence, i.e., a reduced degree of polarization, similar to the loss of coherence in nonseparable quantum systems.

In the future, it will be interesting to extend the concept further to more complex spatio-spectral patterns, e.g., by including spatial Poincaré beams³⁶ or studying SSVBs in the context of optical skyrmions.³⁷ Not only do SSVBs contribute to a better understanding of the complex interplay between different DoFs, they might also enable applications benefiting from the complex correlations and simple generation. In contrast to earlier work, where spatial and spectral vector beams have been used for high-speed tracking of changes in space³⁸ and spectrum,¹⁵ the presented light fields could allow a fruitful combination of the two, leading to novel schemes for advanced sensing methods in all optical domains simultaneously.

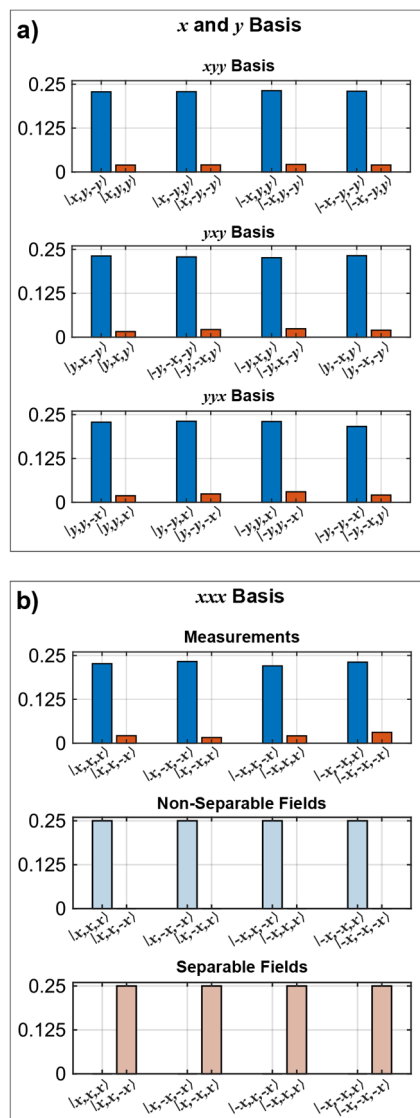


Figure 5. Measurements to show the nonseparability of the SSVB. (a) Measurement probabilities where one DoF is measured in the x basis and the other two are measured in the y basis. The blue bars correspond to the expected states in the mathematical description of a GHZ state, and the red bars correspond to nonexistent states. (b) Measured detection probabilities when all DoFs are measured in the x basis. The measurements in the top row nicely show that the description of the nonseparable state (middle row) is dominant over the expected result for separable fields (lower row).

Furthermore, it will be interesting to study the possible benefits of SSVBs in nonlinear light–matter interactions of structured light.³⁹ This is particularly promising in quantum optical experiments, where the classical correlations of nonseparable light fields can convert to quantum correlations between different photons.⁴⁰ In this regard, the use of SSVBs in the generation of complex entangled states in multiple DoFs is a natural direction for future research.^{41,42} Finally, the similarity of classical nonseparability and quantum entanglement might be beneficially utilized in quantum information applications, as has already been shown for spatial vector beams in quantum communication.⁴³

■ ASSOCIATED CONTENT

SI Supporting Information

The Supporting Information is available free of charge at <https://pubs.acs.org/doi/10.1021/acsp Photonics.3c01322>.

Simulation of the degree of polarization; more details on the analogy to the quantum description (PDF)

■ AUTHOR INFORMATION

Corresponding Authors

Lea Kopf – Photonics Laboratory, Physics Unit, Tampere University, Tampere FI-33720, Finland; orcid.org/0000-0002-7629-0492; Email: lea.kopf@tuni.fi

Rafael Barros – Photonics Laboratory, Physics Unit, Tampere University, Tampere FI-33720, Finland; Email: rafael.barros@tuni.fi

Robert Fickler – Photonics Laboratory, Physics Unit, Tampere University, Tampere FI-33720, Finland; Email: robert.fickler@tuni.fi

Complete contact information is available at:

<https://pubs.acs.org/10.1021/acsp Photonics.3c01322>

Funding

The authors acknowledge the support of the Research Council of Finland through the Photonics Research and Innovation Flagship (PREIN, decision 320165). L.K. acknowledges the support of the Vilho, Yrjö and Kalle Väisälä Foundation of the Finnish Academy of Science and Letters. R.B. acknowledges the support of the Research Council of Finland through the postdoctoral researcher funding (decision 349120). R.F. acknowledges the support of the Research Council of Finland through the Academy Research Fellowship (decision 332399).

Notes

The authors declare no competing financial interest.

Preprint: Lea Kopf; Rafael Barros; Robert Fickler. Correlating space, wavelength, and polarization of light: Spatio-Spectral Vector Beams. 2023, 1007.2528. ArXiv. [10.48550/arXiv.2307.02965](https://arxiv.org/abs/10.48550/arXiv.2307.02965) (accessed November 21, 2023).

■ REFERENCES

- (1) Rubinsztein-Dunlop, H.; et al. Roadmap on structured light. *Journal of Optics* **2017**, *19*, 013001.
- (2) Forbes, A.; de Oliveira, M.; Dennis, M. R. Structured light. *Nat. Photonics* **2021**, *15*, 253–262.
- (3) Piccardo, M.; et al. Roadmap on multimode light shaping. *Journal of Optics* **2022**, *24*, 013001.
- (4) He, C.; Shen, Y.; Forbes, A. Towards higher-dimensional structured light. *Light: Science Applications* **2022**, *11*, 205.
- (5) Shen, Y.; Zhan, Q.; Wright, L. G.; Christodoulides, D. N.; Wise, F. W.; Willner, A. E.; Zou, K.-h.; Zhao, Z.; Porras, M. A.; Chong, A.; et al. Roadmap on spatiotemporal light fields. *Journal of Optics* **2023**, *25*, 093001.
- (6) Wan, Z.; Wang, H.; Liu, Q.; Fu, X.; Shen, Y. Ultra-Degree-of-Freedom Structured Light for Ultracapacity Information Carriers. *ACS Photonics* **2023**, *10*, 2149–2164.
- (7) Weiner, A. M. Femtosecond pulse shaping using spatial light modulators. *Review of scientific instruments* **2000**, *71*, 1929–1960.
- (8) Dickey, F. M. *Laser Beam Shaping: Theory and Techniques*; CRC Press, 2018.
- (9) Chen, L.; Zhu, W.; Huo, P.; Song, J.; Lezec, H. J.; Xu, T.; Agrawal, A. Synthesizing ultrafast optical pulses with arbitrary spatiotemporal control. *Science Advances* **2022**, *8*, eabq8314.

- (10) Jhajj, N.; Larkin, I.; Rosenthal, E. W.; Zahedpour, S.; Wahlstrand, J. K.; Milchberg, H. M. Spatiotemporal Optical Vortices. *Phys. Rev. X* **2016**, *6*, 031037.
- (11) Cao, Q.; Zheng, P.; Zhan, Q. Vectorial sculpturing of spatiotemporal wavepackets. *APL Photonics* **2022**, *7*, 096102.
- (12) Sano, K.; Okada, K.; Hashimoto, K. Simple optical wavelength meter in 700–1200 nm wavelength region. *Electron. Lett.* **1980**, *24*, 912–913.
- (13) del Toro Iniesta, J. C. *Introduction to spectropolarimetry*; Cambridge University Press, 2003.
- (14) Aspnes, D. Spectroscopic ellipsometry—past and future. *Thin Solid Films* **2014**, *571*, 334–344.
- (15) Kopf, L.; Ruano, J. R. D.; Hiekkamäki, M.; Stolt, T.; Huttunen, M. J.; Bouchard, F.; Fickler, R. Spectral vector beams for high-speed spectroscopic measurements. *Optica* **2021**, *8*, 930–935.
- (16) Jolly, S. W.; Gobert, O.; Quéré, F. Spatio-spectral characterization of ultrashort laser pulses with a birefringent delay line. *OSA Continuum* **2021**, *4*, 2044–2051.
- (17) Holleczeck, A.; Aiello, A.; Gabriel, C.; Marquardt, C.; Leuchs, G. Poincaré sphere representation for classical inseparable Bell-like states of the electromagnetic field. *arXiv* **2010**, 1007.2528 (accessed on 21.11.2023).
- (18) Milione, G.; Sztul, H. I.; Nolan, D. A.; Alfano, R. R. Higher-Order Poincaré Sphere, Stokes Parameters, and the Angular Momentum of Light. *Phys. Rev. Lett.* **2011**, *107*, 053601.
- (19) See the Supporting Information.
- (20) Bouwmeester, D.; Pan, J.-W.; Daniell, M.; Weinfurter, H.; Zeilinger, A. Observation of three-photon Greenberger-Horne-Zeilinger entanglement. *Phys. Rev. Lett.* **1999**, *82*, 1345.
- (21) Pan, J. W.; Bouwmeester, D.; Daniell, M.; Weinfurter, H.; Zeilinger, A. Experimental test of quantum nonlocality in three-photon Greenberger-Horne-Zeilinger entanglement. *Nature* **2000**, *403*, 515–519.
- (22) Greenberger, D. M.; Horne, M. A.; Zeilinger, A. In *Bell's Theorem, Quantum Theory and Conceptions of the Universe*; Kafatos, M., Ed.; Springer Netherlands: Dordrecht, 1989; pp 69–72.
- (23) Zhan, Q. Cylindrical vector beams: from mathematical concepts to applications. *Adv. Opt. Photon.* **2009**, *1*, 1–57.
- (24) Balthazar, W. F.; Souza, C. E. R.; Caetano, D. P.; Galvao, E. F.; Huguenin, J. A. O.; Khoury, A. Z. Tripartite nonseparability in classical optics. *Opt. Lett.* **2016**, *41*, 5797–5800.
- (25) Biener, G.; Niv, A.; Kleiner, V.; Hasman, E. Formation of helical beams by use of Pancharatnam–Berry phase optical elements. *Opt. Lett.* **2002**, *27*, 1875–1877.
- (26) Monmayrant, A.; Weber, S.; Chatel, B. A newcomer's guide to ultrashort pulse shaping and characterization. *Journal of Physics B: Atomic, Molecular and Optical Physics* **2010**, *43*, 103001.
- (27) Spreuw, R. J. C. A Classical Analogy of Entanglement. *Foundations of Physics* **1998**, *28*, 361–374.
- (28) Aiello, A.; Töppel, F.; Marquardt, C.; Giacobino, E.; Leuchs, G. Quantum-like nonseparable structures in optical beams. *New J. Phys.* **2015**, *17*, 043024.
- (29) Shen, Y.; Nape, I.; Yang, X.; Fu, X.; Gong, M.; Naidoo, D.; Forbes, A. Creation and control of high-dimensional multi-partite classically entangled light. *Light Sci. Appl.* **2021**, *10*, 50.
- (30) Karimi, E.; Boyd, R. W. Classical entanglement? *Science* **2015**, *350*, 1172–1173.
- (31) Töppel, F.; Aiello, A.; Marquardt, C.; Giacobino, E.; Leuchs, G. Classical entanglement in polarization metrology. *New J. Phys.* **2014**, *16*, 073019.
- (32) Allen, L.; Beijersbergen, M. W.; Spreuw, R. J. C.; Woerdman, J. P. Orbital angular momentum of light and the transformation of Laguerre-Gaussian laser modes. *Phys. Rev. A* **1992**, *45*, 8185–8189.
- (33) Padgett, M. J.; Courtial, J. Poincaré-sphere equivalent for light beams containing orbital angular momentum. *Optics letters* **1999**, *24*, 430–432.
- (34) Fickler, R.; Lapkiewicz, R.; Plick, W. N.; Krenn, M.; Schaeff, C.; Ramelow, S.; Zeilinger, A. Quantum entanglement of high angular momenta. *Science* **2012**, *338*, 640–643.
- (35) Plick, W. N.; Fickler, R.; Lapkiewicz, R.; Ramelow, S. Violation of an extended Wigner inequality with high-angular-momentum states. *Phys. Rev. A* **2015**, *91*, 022124.
- (36) Beckley, A. M.; Brown, T. G.; Alonso, M. A. Full Poincaré beams. *Opt. Express* **2010**, *18*, 10777–10785.
- (37) Shen, Y.; Martínez, E. C.; Rosales-Guzmán, C. Generation of Optical Skyrmions with Tunable Topological Textures. *ACS Photonics* **2022**, *9*, 296–303.
- (38) Berg-Johansen, S.; Töppel, F.; Stiller, B.; Banzer, P.; Ornigotti, M.; Giacobino, E.; Leuchs, G.; Aiello, A.; Marquardt, C. Classically entangled optical beams for high-speed kinematic sensing. *Optica* **2015**, *2*, 864–868.
- (39) Buono, W. T.; Forbes, A. Nonlinear optics with structured light. *Opto-Electronic Advances* **2022**, *5*, 210174-1–210174-19.
- (40) Khoury, A. Z.; Souto Ribeiro, P. H.; Dechoum, K. Transfer of angular spectrum in parametric down-conversion with structured light. *Phys. Rev. A* **2020**, *102*, 033708.
- (41) Barreiro, J. T.; Langford, N. K.; Peters, N. A.; Kwiat, P. G. Generation of Hyperentangled Photon Pairs. *Phys. Rev. Lett.* **2005**, *95*, 260501.
- (42) Achatz, L.; Bulla, L.; Ecker, S.; Ortega, E. A.; Bartokos, M.; Alvarado-Zacarias, J. C.; Amezcua-Correa, R.; Bohmann, M.; Ursin, R.; Huber, M. Simultaneous transmission of hyper-entanglement in three degrees of freedom through a multicore fiber. *npj Quantum Information* **2023**, *9*, 45.
- (43) Ndagano, B.; Perez-Garcia, B.; Roux, F. S.; McLaren, M.; Rosales-Guzman, C.; Zhang, Y.; Mouane, O.; Hernandez-Aranda, R. I.; Konrad, T.; Forbes, A. Characterizing quantum channels with non-separable states of classical light. *Nat. Phys.* **2017**, *13*, 397–402.